Thermal and electrical transport in ZrB2-SiC-WC ceramics up to 1800 °C

Ma, Hai-bin; Zou, Ji; Zhu, Jing-ting; Lu, Ping; Xu, Fangfang; Zhang, Guojun

DOI:
10.1016/j.actamat.2017.02.052

Document Version
Peer reviewed version

Citation for published version (Harvard):
Ma, H, Zou, J, Zhu, J, Lu, P, Xu, F & Zhang, G 2017, 'Thermal and electrical transport in ZrB2-SiC-WC ceramics up to 1800 °C', *Acta Materialia*, vol. 129, pp. 159-169. https://doi.org/10.1016/j.actamat.2017.02.052

Accepted Manuscript

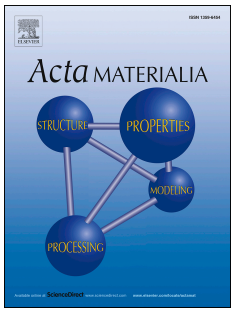

Thermal and electrical transport in ZrB_2-SiC-WC ceramics up to 1800^{o}C

Hai-Bin Ma, Ji Zou, Jing-Ting Zhu, Ping Lu, Fang-Fang Xu, Guo-Jun Zhang

PII: S1359-6454(17)30153-2

DOI: 10.1016/j.actamat.2017.02.052

Reference: AM 13580

To appear in: *Acta Materialia*

Please cite this article as: Hai-Bin Ma, Ji Zou, Jing-Ting Zhu, Ping Lu, Fang-Fang Xu, Guo-Jun Zhang, Thermal and electrical transport in ZrB_2-SiC-WC ceramics up to 1800^{o}C, *Acta Materialia* (2017), doi: 10.1016/j.actamat.2017.02.052

Thermal and electrical transport in ZrB_2-SiC-WC ceramics up to 1800^{o}C

Hai-Bin Ma[a,c,d#], Ji Zou[b,#,*], Jing-Ting Zhu[c,d], Ping Lu[c] ,Fang-Fang Xu[c] and Guo-Jun Zhang[a,c*]

[a] State Key Laboratory for Modification of Chemical Fibers and Polymer Materials, Institute of Functional Materials, Donghua University, Shanghai, 201620, China.
[b] School of Metallurgy and Materials, University of Birmingham, B15 2TT, UK.
[c] State Key Laboratory of High Performance Ceramics and Superfine Microstructure, Shanghai Institute of Ceramics, Chinese Academy of Sciences, Shanghai 200050, China.
[d] University of Chinese Academy of Sciences, Beijing 100049, China.

[#] Haibin and Ji contributed equally to this work.
*Corresponding author, email: zouji1983@gmail.com; zouji1983@aliyun.com; gjzhang@dhu.edu.cn.

Abstract

The thermophysical properties of dense ZrB_2-20 vol.% SiC ceramics (ZS) with and without doping of 5 vol.% WC (ZSW) were characterized up to 1800^{o}C. Because of the in-situ formed WB with low thermal conductivity and the strong phonon scattering effect from $(Zr,W)B_2$ solid solution, the thermal conductivity of ZSW (36.2 W/(m·K)) at room temperature is much lower than that of ZS (100.4 W/(m·K)), however, their differences at 1800^{o}C is very limited (42.2 W/(m·K) for ZSW and 47.4 W/(m·K) for ZS). The detailed calculation indicates that contributions from lattice vibrations on the thermal conductivity decreased to nearly zero at 1800^{o}C in both samples, therefore, electrical conductivity of ZS and ZSW dominates their thermal transport behavior at higher temperatures. Furthermore, amorphous phase with compositions of Ca-Al-Si-O was occasionally found at the triple junction of ZS, its softening and rewetting of the grain boundary at higher temperature were confirmed from the internal friction curve and microstructural characterization at different levels, which was thought to be responsible for the tremendous increase of Interfacial thermal resistance and continuous drop of thermal conductivity of ZS up to 1800^{o}C. On the contrary, benefiting from the clean boundary and tight triple junction in ZSW, its thermal conductivity can stabilize between 36 and 47 W/(m·K) in a broad temperature range from 25 to 1800^{o}C. Based on the

measurement above, the type of carriers and thermoelectric figure of merit (*zT*) in ZrB_2-SiC based ceramics are also firstly reported.

Key words: Borides; UHTCs; Thermal conductivity; Microstructures; Internal friction

1. Introduction

Rapid development of hypersonic vehicles makes the world shrink. However, serious aero-heating during hypersonic flight (>Mach 5) inevitably results in the fast temperature increase up to >2000^{o}C on the sharp leading edge and nose cone of the aircraft in few minutes. Unfortunately, conventional active or semi-passive cooling is impractical on these components due to the constraints from aerodynamic shape [1]. Therefore, ablation-resistant materials with high thermal conductivity are desired and currently being considered for these applications. Moreover, the materials with high thermal conductivity also exhibit better thermal shock resistance (TSR). Good TSR is particularly demanding for the thermal protection part on the hypersonic vehicle, which has to withstand rapid changes in temperature. Ultra-high temperature ceramics (UHTCs), such as ZrB_2 and HfB_2, possess a unique combination of high thermal conductivity, high melting temperature and relatively good mechanical properties, making them ideal for aforementioned applications [2-5].

ZrB_2-SiC-WC is an emerging material system among UHTCs. WC has been proved to play a positive role on improving the densification [6], fracture toughness [7] and oxidation resistance of ZrB_2-SiC ceramics [8]. More important, ZrB_2 based ceramics with WC additions (ZSW) showed excellent high-temperature strength in both argon and air atmosphere [9-11], no strength degradation was detected in its bending strength up to 1600^{o}C. However, the effect of WC on the thermophysical properties, especially on the high-temperature thermal conductivity of ZrB_2-SiC ceramics hasn't been well explored. Recently, McClane *et al.* [12] investigated the thermal properties of $(Zr,W)B_2$ solid solution, but the temperature range in their work was limited from 25 to 200^{o}C, which is far from the real condition a hypersonic flight will experience.

For multiphase ceramics with a continuous major phase, the effective thermal conductivity could be given by Maxwell's equation and its corrections

[13]. Nevertheless, as a result of the complicated chemical reactions and possible solid solution of W into ZrB_2 lattice [14,15], the thermal conductivity of ZSW couldn't be simply predicted, even at room temperature. Therefore, the goal of this work is to investigate the thermal and electrical characteristic of dense ZrB_2-SiC (ZS) and ZrB_2-SiC-WC (ZSW) ceramics up to 1800^{o}C and relate the thermophysical performance of these ceramics to their features, e.g. microstructure and internal friction behavior. Based on these results, a new mechanism for realizing a high thermal conductivity in ZSW ceramics at 1800^{o}C will be presented; the thermoelectric figure of merit (*zT)* of ZrB_2-SiC based UHTCs will also be firstly reported.

2. Experimental procedures

Self-synthesized ZrB_2 powder (D_{50}=1.05 μm, purity 98%, O 0.46 wt.%), commercial α-SiC (D_{50}=0.45 μm, purity 98.5%, Changle Xinyuan Carborundum Micropowder Co. Ltd., China) and WC powder (D_{50}<1 μm, Hard alloy Co., Ltd., Zhuzhou, China) were chosen as the starting materials. ZrB_2 powder was synthesized through a boron/carbothermal reaction between ZrO_2 and B_4C in vacuum [16]. An appropriate amount of each powder was blended to prepare 80 vol.% ZrB_2 and 20 vol.% SiC for ZS and 80 vol.% ZrB_2, 20 vol.% SiC and additional 5 vol.% WC for ZSW. As prepared powder mixtures were mixed in ethanol for 24 h in a polyethylene jar using Si_3N_4 balls, following by drying them through a rotary evaporation at 70^{o}C in mild vacuum. As dried powders were first sieved through a 200-mesh screen, then were poured into a graphite die (37×30 mm) lined with spray-coated h-BN. The mixtures were heated to 1600ºC and held at this temperature for 30 min, thereafter a pressure of 30 MPa was applied on the sample gradually, and meanwhile the furnace was backfilled with argon gas. Finally, the samples were densified at 2000ºC for 1h.

The density of as sintered samples was measured by the Archimedes method in deionized water. The phase constitution and lattice parameters on the sintered ceramics were determined by X-ray diffraction analysis (XRD, D/Max-2250V, Rigaku, Tokyo, Japan). Vegard's law (Eq. (1)) was used to calculate the averaged W content in (Zr,W)B_2 solid solution.

$$C_{W\,in\,Zr(W)B_2} = \frac{A_{ZrB_2} - A_{Zr(W)B_2}}{A_{ZrB_2} - A_{WB_2}} \times 100\% \quad (1)$$

The internal friction or damping behavior of ZS and ZSW samples up to 1500^{o}C was measured by suspending the sample in a graphite heating furnace through an impulse excitation technique (IET) [17-19]. For all the experiments, tests were performed in a static argon atmosphere and the heating/cooling rate of the furnace was set as 3^{o}C/min. Rectangular bar with a dimension of 6mm (width) ×1.5mm (thickness) ×40mm (length) was excited twice in one minute by an impact of an Al_2O_3 projectile. The vibration signals were then collected through a bottom placed microphone. Resonance frequencies (f_r) could be extracted by analyzing the signals. The damping value (Q^{-1}) can be calculated from Eq. (2) with a decay parameter K.

$$Q^{-1} = K / \pi \cdot f_r \quad (2)$$

Grazing incidence diffraction (GIXD, 3003-TT, Seifert, Ahrensburg, Germany) with a series of incident angles from 0.5 to 3 degree was collected on the surface of a ZSW bar, which had been tested by IET, using Cu Kα radiation at 40 kV and 40 mA.

Microstructures and compositions on the polished ZS and ZSW ceramics were observed via scanning electron microscope (SEM, Magellan 400, FEI, USA) with energy dispersive spectroscopy (EDS, X-Max 80T, Oxford, UK). The element mapping on the polished cross section of the sample after IET test was performed by electron probe microanalysis (EPMA; JXA-8530F, JEOL, Tokyo, Japan).High resolution images of the grain boundary structures in ZS and ZSW were analyzed through transmission electron microscope (TEM, Tecnai F20, FEI Corp), which was carried out at 200kV. At least 8 grain boundaries in each specimen were randomly checked and analyzed. Scanning transmission electron microscopy (STEM) images, elemental line scan, EDS and electron energy loss spectrometry (EELS, GIF 963, Gatan, USA) were performed by a JEOL TEM (JEM-2100F, Japan). EDS and EELS were combined to detect the composition of the glassy phase located at the triangular grain boundary of thin ZS slice.

Thermal diffusivity was measured via laser flash measurement (LFA) on pellets with dimensions of Φ10 mm (diameter) ×3 mm (thickness) in a graphite furnace in flowing argon. Before carrying out a FLA measurement, a thin graphite coating (~50 μm) was sprayed on the surface of the pellet to improve its emission/absorption property. The lower surface of the sample was irritated by a laser (100mW) with an energy pulse of 200ms, thereafter, the

temperature change on the upper surface of the sample was recorded every 100^{o}C up to 1800^{o}C. Diffusivity value was calculated by fitting the recorded curve with a Cowen's correction to account the heat loss from convection and radiation [20], each diffusivity value reported was averaged from at least three measurement and the deviation is less than 0.002 cm^2/s. Thermal capacity of ZSW and ZS was measured on cylinders with dimensions of Φ5 mm×18 mm by drop calorimetry (MHTC 96, Setaram Inc., France). Then, the thermal conductivity of ZS and ZSW ceramics were calculated according to diffusivity (*α)*, capacity (c_p*)* and density values (*ρ)* (Eq. (3)).

$$\lambda = \rho \alpha c_p \quad (3)$$

For electrical transport, bars with dimensions of 2 mm × 2 mm × 8 mm were chosen to measure its electrical properties through a Seebeck coefficient/electric resistance measuring system (ZEM-3, ULVAC, US). The energy conversion efficiency is generally evaluated by the dimensionless thermoelectric figure of merit (*zT*) through Eq. (4):

$$zT = \frac{S^2 \sigma T}{\kappa} \quad (4)$$

where *S* is the Seebeck coefficient, *σ* is the electrical conductivity, *T* is the absolute temperature, and *λ* is the thermal conductivity.

3. Results

3.1 Overall microstructure

The measured densities of ZS and ZSW are 5.55 and 6.04 g/cm^3, respectively. No obvious pores can be found on their polished surfaces (Fig. 1), implying a high relative density has been achieved. From Fig. 1b and corresponding EDS results of grains with different contrasts in ZSW, it can be found that apart from ZrB_2 (gray) and SiC (black), WB (bright white) and ZrC (dark white), instead of WC additions, were found on ZSW because of the reactions between WC, ZrO_2 and ZrB_2 [10,11,15]. Because of the Zener pinning effects from the in-situ formed WB and ZrC with fine grains, an obvious refinement on ZrB_2 grains was detected in ZSW, i.e. the averaged grain size of ZrB_2 in ZSW is 1.0±0.4 μm, which is almost half of that in ZS (1.9±0.8 μm). In addition, peak shift of ZrB_2 towards higher angles was found in the diffraction

pattern of ZSW (Fig. 2b), implying that some W atoms have been incorporated into ZrB_2 lattices during sintering. This also has been supported by the EDS results (Fig. 1) in ZSW. According to the XRD results, lattice parameters of ZrB_2 in ZSW were calculated to be a=b=3.16407 Å and c=3.52311 Å. Thereafter the averaged W content in $(Zr,W)B_2$ solid solution is calculated to be 3.1 at.% by the Vegard's law.

3.2 TEM Observation

A representative high angle annular dark field (HAADF) image of ZS is displayed in Fig. 3a, SiC and ZrB_2 grains could be easily recognized through their contrasts. From this image, it also clear that at some triple junctions, the contrast is a bit darker compared to the ZrB_2 and SiC grains adjacent (as circled in 3a). A combined EDS and EELS analysis (Fig. 3b and c) revealing that this impurities normally include Si, Ca, Al, O, C, but in some rare cases, F, Mg, Zr and Y could also be detected. The EDS mapping of some major impurity elements (Fig. 3f) proves that their distributions on this phase are homogenous. Its corresponding HRTEM image is shown in Fig. 3g, demonstrating a typical amorphous nature of that phase.

HRTEM images of typical grain boundaries (GBs) in ZS and ZSW are shown in Fig. 3i and h, respectively. Both of them look clean and neighboring grains are directly bonded. EELS line scans in ZSW also verified that no oxygen impurities aggregated in the GBs. However, in ZS, although most the analyzed GBs are free of O, we did find trace oxygen gathered at the boundary between SiC and ZrB_2 or SiC and SiC grains, nevertheless, this phenomenon only occurs in the position near to the glassy phase (Fig. 3d and e).

3.3 Thermal properties

Plots depicting the variations of thermal diffusivity, specific heat capacity and thermal conductivity as a function of the temperature for both ZS and ZSW are presented in Fig. 4. For ZS, its thermal diffusivity has the maximum value at room temperature (RT) and decreased exponentially to its minimum value at 1800^{o}C. As regards to ZSW, however, the thermal diffusivity drops linearly with the temperature increase. Although the thermal diffusivity of ZS at RT is 0.36 cm^2/s, nearly twice than that the corresponding value in ZSW, their values approached to a similar level at 1800^{o}C, i.e. 0.10 and 0.09 cm^2/s for ZS and

ZSW, respectively. The Debye temperature (T_θ) for ZrB_2 has been reported to 500~858^{o}C [21]. Above T_θ, materials with higher thermal diffusivity normally own a larger thermal conductivity. The similar diffusivity value between ZS and ZSW at 1800^{o}C is the first indication that their thermal conductivity will approach a similar level at enough high temperatures [22].

To convert thermal diffusivity to conductivity, it is necessary to know the specific heat (c_p) at elevating temperatures, in addition to the density of ZS and ZSW. Herein, the density of ZS and ZSW was considered as a constant irrelevant with the temperature, in view of the limited thermal expansion on ceramics. Although Kopp–Neumann's law could be used to estimate the specific heat capacity of the composite based on the c_p value and amount of each component, some errors may occur in our case. For example, WC will be consumed by a series of oxygen removing reactions in ZrB_2 matrix, consequently, the exact amount of reaction products, i.e. WB and ZrC, are hard to be estimated. Also K-N relationship didn't match very well with the experiments when the solid solution becomes significant. For this purpose, specific heat capacity of ZS and ZSW were measured accurately by drop calorimetry, the corresponding values were recorded in Fig. 4b.

The minimum specific heat capacity of 0.50 J/(g·K) for ZS was measured at RT, and its value increased with temperature to the maximum of 0.81 J/(g·K) at 1400^{o}C. The measured c_p of ZS is higher than that in ZSW throughout the temperature range and both of them exhibit a similar tendency as temperature increase (Fig. 4b). It is also observed that the c_p of ZS and ZSW rises sharply below ~600^{o}C, in accordance with the T_θ of ZrB_2. Above the temperature, the growth of c_p becomes slowly towards the limitation (75 J/(mol·K) or 0.67 J/(g·K) for ZrB_2) predicted by the Dulong–Petit law. The calculated specific heat capacity by summing up the c_p of each component in ZS and ZSW from the database of HSC Chemistry 6 (Outokumpu Research Oy, Pori, Finland) is added in Fig. 4b for a comparison. Although the calculated curves exhibit a similar shape to those had been measured, the difference, especially for the values at lower temperature, is obvious: the measured value is ~10% larger than the one calculated by the mixing rule.

ZS ceramics have the highest thermal conductivity with a value of 100.4 W/(mK) at RT, which sharply dropped to ~ 60 W/(m·K) at 800^{o}C and then gradually decreased to 47.7 W/(m·K) at 1800^{o}C. For ZSW, its thermal

conductivity increased from 36.2 to 45.1 W/(m·K) initially from RT to 300^{o}C, then the value stabilized at ~45 W/(m·K), with little variations between 300^{o}C and 1400^{o}C. Further increase the temperature, a linear drop in thermal conductivity was found between 1400 and 1800^{o}C. It is worthwhile to mention that the thermal conductivity of ZSW at 1800^{o}C (42.4 W/(mK)) is slightly higher than that at room temperature (36.2 W/(m·K)). Furthermore, the thermal conductivity of ZSW can fluctuate in a narrow zone between 36 and 47 W/(m·K) in a broad temperature from 25 to1800^{o}C, this aspect will be particularly useful for some engineering designs. Although the calculated λ for ZS at RT is slightly higher than that in the literature, its temperature dependence fits well with the trends previously reported [23]. The remarkable difference on the thermal conductivity between ZS and ZSW will be further addressed in 4.1.

3.4 Electrical and thermoelectrical properties

The electrical resistance values of ZS and ZSW were measured from room temperature to 700^{o}C. Electrical resistivity increases linearly with increasing temperature for both of these two samples which fits with a previous investigation of ZrB_2-SiC composites [24]. For higher temperature, electrical resistance values were estimated by a linear extrapolation to 1800^{o}C [24], as shown in Fig. 5a. At room temperature, electrical conductivity of ZS (8.13×10^6 S/m) is much higher than that of ZSW (2.42×10^6 S/m) (Fig. 5a). However, electrical conductivity value of ZS decreases significantly as temperature increasing. The gap between ZS and ZSW becomes smaller as temperature increasing, at 1800^{o}C, their difference is 0.23 $\times10^6$ S/m.

The temperature dependence of Seebeck coefficients (*S*) were measured for ZS and ZSW (Fig. 5b), both of the values are negative. The negative *S* values indicate that electron-like behavior predominates the electrical transport in diborides. As a semiconductor, α-SiC has much higher Seebeck coefficient which was reported to be ~340 μV/K at room temperature [25]. However, 20 vol.% SiC addition doesn't seem to increase the Seebeck value of ZS, -4 μV/K measured in ZS at RT is close to the value of pure ZrB_2 [26]. *zT* values of ZS and ZSW ceramics all increased when elevating the temperatures. The absolute Seebeck coefficient of ZSW is lower than that of ZS in the measured range. The *zT* of ZS is slightly higher than that of ZSW (Fig. 5c) up on 500^{o}C.

At 500^{o}C, the *zT* value of ZS is 0.02. A recent report showing that the Seebeck coefficient of boron rich boride (ZrB_{12}) ceramics is positive [27]. The combination of positive and negative Seebeck coefficient in Zr-B system implies that it is possible to construct thermoelectric circuit by only conductive borides, although the low *zT* value demonstrates that a huge effort is needed for exploiting their thermoelectric effect into any practical applications.

3.5 Internal friction of ZS and ZSW

As observed in the other ceramics, the damping curves of both ZS and ZSW show an exponential increase with temperature during heating and cooling, due to a suppression of the relaxation resulting from grain-boundary sliding. In ZS, three distinct peaks, centered at 790^{o}C, 1000^{o}C and 1200^{o}C were found separately upon heating, whereas only the P1 peak is visible when temperature cooled down. Intrinsically, the damping peak must be originated from an anelastic relaxation processes, e.g. phase transformation, defect migration and chemical reactions. Apparently, the phenomenon behind peak P1 should be reversible during the thermal cycles, while the relaxation process for peak P2 and P3 is irreversible.

For ZSW, two extra peaks superposed on an exponential-like background were observed during heating, their shape and position are analogous to P2 and P3 in ZS. However, these peaks exhibits relatively lower intensity and a small shift between P2 (P3) and P2' (P3') were also identified (Fig. 6a). Likewise, P2' and P3' couldn't be detected on the cooling curve of ZSW.

4. Discussion

4.1 The contribution of electron and phonon on the thermal conductivity

The total thermal conductivity (λ_{total}) for conductive boride ceramics is equal to the sum of the contributions from electron (λ_e) and phonon (λ_{ph}):

$$\lambda_{total} = \lambda_e + \lambda_{ph} \quad (5)$$

Here, λ_e was calculated from the electrical conductivity (as shown in Fig. 5(a)) using the Wiedemann-Franz law (Eq. (6)), where σ is the electrical conductivity, *T* is the absolute temperature and *L* is the Lorentz constant that can be calculated according to Eq. (7). λ_{ph} was then calculated by subtracting the

electron contribution from its total thermal conductivity. Fig. 4c and d illustrate the variations of electron and phonon contributions to thermal conductivity as a function of temperatures for ZS and ZSW ceramics.

For ZS ceramics, λ_e is not very sensitive to the change of temperatures while λ_{ph} decreases remarkably with T increases. When temperature reached 1500℃, λ_{ph} is lower than zero. Obviously, negative phonon contributions are not physically possible. The reason is that the Lorenz number for ZrB_2 with additives must have a smaller value than 2.44×10^{-8} WΩK^{-2}. The true Lorenz number was calculated by solving Boltzmann transport equation, which involves the contribution from Boltzmann constant (k_b), electron charge (e), scattering parameter (r) and reduced Fermi energy [28]. Among these, k_b and *e* are known parameters *and* r depends on the scattering mechanism for the main carriers in ZS and ZSW, and acoustic phonon scattering was assumed here. The calculation of reduced Fermi energy can be derived from as measured Seebeck coefficients by solving the Fermi integral. Thus, the temperature dependence of realistic Lorenz numbers for ZS and ZSW could be calculated as plotted in Fig. 6. At room temperature, true Lorenz number is close to the classical value of 2.44×10^{-8} WΩK^{-2} for both samples. However, the calculated values decrease nonlinearly with the increasing of temperature. Due to the limitation on our ZEM system, L can only be calculated up to 500^{o}C. If the L value calculated at 500^{o}C (2.39×10^{-8} WΩK^{-2}) was chosen for calculating λ_{ph}, λ_{ph} at 1500^{o}C will be above zero (0.91 W/(m·K)). Since the Debye temperature for ZrB_2 is larger than 500^{o}C [21], an even larger L value is expected at 1500^{o}C and above. Accordingly, λ_{ph} value for ZS should be positive in the whole temperature range. Although the value of λ_{ph} is not absolutely accurate on the grounds of the fixed Lorenz number value used in Fig.5, it still can be concluded that the contributions from phonon become much weaker at higher temperatures since the deviation of L was proven to be small (Fig.6) [29]. For ZSW ceramics, λ_e increased continuously from 17.6 to 40.3 W/(m·K) from RT to 1800^{o}C, meanwhile, λ_{ph} increased a little bit from RT to 200^{o}C and then decreased linearly as temperature goes up further. At 1800^{o}C, λ_{ph} in ZSW is also approaching zero (2.02 W/(m·K)).

$$\lambda_e = L\sigma T \quad (6)$$

$$L = \frac{\pi^2 k_B^2}{3e^2} = 2.44\times10^{-8}(\mathrm{W\Omega K^{-2}}) \quad (7)$$

Both of λ_e and λ_{ph} are associated with the heat capacity (C_i), velocity (v_i) and the mean free path (l_i) of corresponding carriers (i) (Eq. 8).

$$\lambda = \sum_{i=e,ph} \frac{1}{3} C_i v_i l_i \quad (8)$$

For phonon contributions, l_{ph} is mainly generated by two types of scattering processes, namely, geometric scattering and phonon-phonon scattering. In fact, l_{ph} is dominated by the shortest mean free path during scattering. For geometric scattering, the value sharply decreases from the distance between neighboring grains at lower temperature to few lattices at moderate temperature, further keeps this value at higher temperature. In contrast, the phonon-phonon scattering is reversely proportional to the temperature in inharmonic lattices. Phonon velocity (v_{ph}) is determined by the stiffness and density of the solids, both of which are affected by the temperature, but are insignificant. Therefore, v_{ph} can be considered as a constant, irrelevant with temperature. If l_{ph} was governed by geometric scattering, i.e., λ_{ph} should approach a constant value at high temperature, which is not of our case (Fig. 4 c and d). Therefore, phonon-phonon scattering must exist in both of ZS and ZSW, resulting in the continuously drop of λ_{ph} at higher temperatures. Clearly, electron contribution plays an important role on the heat transfer process at higher temperature in this study. In fact, it becomes the only mechanism working in ZS and ZSW at 1800^{o}C. As a result, temperature dependence of electrical conductivity is a crucial parameter to predict and screen borides based UHTCs out for achieving excellent high temperature thermal conductivity.

4.2 Correlation of thermal properties with microstructure

As the discussion above attests, the lower thermal conductivity in ZSW at room temperature is caused by the smaller contributions from both of electrons and lattices; however, the reason for the drop of λ_p and λ_e when WC was added is still unclear. For solving this, the Brick Layer Model (BLM) was employed to figure out the average internal interfacial electrical and thermal resistance in ZS and ZSW. [30,31]:

$$C = (\frac{1}{C_{\text{int}}} + \frac{R}{d})^{-1} \quad (9)$$

$$\sum_{i=1}^{N} \frac{C - C_i}{2C + C_i} f_i = 0 \quad (10)$$

where C is either electrical conductivity (σ) or thermal conductivity (λ) of the matrix phase in composite materials (ZrB_2 phase in this work). C_{int} is the intrinsic electrical or thermal conductivity of the matrix phase, R is the average interfacial electrical or thermal resistance, d is the average matrix grain size. The value of C can be obtained using the effective medium approximation (Eq. 10). Where C_i and f_i are the electrical or thermal conductivity and the volume fraction of the i^{th} phase in composites. For completing these calculations, the intrinsic electrical (σ_{int}) or thermal conductivity (λ_{int}) values for different phases have to be known and were listed in Table I. The calculated interfacial electrical resistances (R_σ) for ZS and ZSW at room temperature are shown in Table II. Although the electrical resistance of ZS is obviously lower than that of ZSW, the differences between their interfacial electrical resistances are unremarkable. In view that the electrical conductivity of ZSW was determined by the conductivity in both of grain and interface, this observation indicates the smaller electrical conductivity in ZSW mainly attributes to the lower conductivity in its grains, i.e. the formation of solid solution of W in ZrB_2. Interfacial thermal resistance of ZSW (1.3×10^{-9} m^2K/W) is nearly 2.4 times larger than that of ZS (5.5×10^{-10} m^2K/W) at room temperature. Considering the thermal conductivity of WB is much lower than that of ZrB_2 and SiC, the thermal resistances of grain boundaries of ZrB_2/WB, ZrB_2/WB and ZrC/WB must be large. Therefore, there are two reasons for explaining the decrease of thermal conductivity with the addition of WC. One is the solid solution of W into ZrB_2 and the another one is the high interfacial thermal resistance in ZSW at RT.

Table I. Electrical and Thermal conductivity values of ZrB_2, SiC, ZrC and WB.

	T(℃)	ZrB_2	SiC	ZrC	WB
σ_{int} (S/m)	RT (25)	2.17×10^7 [32]	2.00×10^4 [33]	2.04×10^6 [34]	5.83×10^5 [35]
λ_{int} (W/mK)		140 [32]	114 [36]	20.5 [37]	0.79*
λ_{int} (W/mK)	1800	58.9 [24]	29.8 [38]	43.7[39]	0.33**

* Measurement of WB bulk sintered via reactive hot pressing using W and B

powders as raw materials.

** Calculated according to the trend of λ_{int} value for ZrB_2.

Table II. Interfacial electrical (R_σ) and thermal (R_λ) resistance of ZS and ZSW.

	T/℃	ZS	ZSW
R_σ / ($\Omega \cdot m^2$)	RT (25)	3.9×10^{-14}	3.1×10^{-14}
R_λ / (m^2K/W)	RT (25)	5.5×10^{-10}	1.3×10^{-9}
	1800	4.2×10^{-9}	3.9×10^{-9}

4.3 Correlation of interfacial thermal resistance and microstructure with damping properties

4.3.1 Understanding the damping peaks in ZS and ZSW

By converting applied vibration energy into the internal energy of a solid body, damping (internal friction) is a measure of the energy dissipation on the sample where a small cyclic stress is applied. Any time dependent self-adjustment of a thermodynamic system towards a new equilibrium state (e.g. the movement of point defects, dislocations, grain boundaries and phase transitions etc.), could be reflected by the damping curves. Hence, the glass transition of amorphous Ca-Si-Al-O should be detectable from Fig. 7 as well. Considering the documented transition temperature for $CaO\text{-}SiO_2\text{-}Al_2O_3$ glass was 750°C-900°C and P1 peak in ZS was centered also at this temperature range, the relaxation process of P1 was probably caused by the glass transition. Interestingly, P1 was also found in ZS during cooling and located at nearly the same place as heating. It reveals that the crystallization of glass melt didn't take place on the amorphous $CaO\text{-}SiO_2\text{-}Al_2O_3$ up to 1500°C in our system; at least, they were not fully crystallized.

The next task is to interpret the formation of P2 (P2') and P3 (P3') in ZS and ZSW. Since both of them are irreversible and existed in all the samples, we hypothesize that these peaks are related with a surface degradation process of the samples during the IET tests. For verifying this, one ZSW sample after IET was carefully polished (Fig. 8), its cross section clearly showed an extra contaminated layer with an averaged depth of 11 μm. The elemental mapping by WDS confirmed that this boron and silicon depleted layer is rich in O and Zr, although a carbon-containing zone was also observed. GIXRD results with different incident angles from 0.5 to 3 degree are shown in

Fig. 9. The phase assemblage on this oxidation layer mainly contains m-ZrO_2 and ZrC. It seems that more ZrC phase existed in the area near the unreacted samples, as suggested by comparing the peak intensity between ZrC and ZrO_2 at different incident angles. Building on these observations, the oxidation of SiC and the carbonization/oxidation of ZrB_2 must occur during the long IET runs (~13 h) in graphite furnace (Reactions 11-13), and obviously, the occurrence of a carbonization process of ZrB_2 was prior to its oxidation.

$$SiC + O_2(g) = SiO(g) + CO(g) \quad (11)$$

$$ZrB_2 + C + O_2(g) = ZrC + CO(g) + B_2O_3 \quad (12)$$

$$2ZrC + 3O_2(g) = 2ZrO_2 + 2CO(g) \quad (13)$$

Evidently, P2 and P3 should originate from these irreversible reactions. The slightly difference of positions on these two peaks in ZS and ZSW suggests that the incorporation of WB in ZS influence the starting oxidation/ carbonization temperature for both of ZrB_2 and SiC, the detailed work to separate these peaks from different reactions is still underway.

4.3.2 Rewetting the grain boundary at higher temperature

Interfacial thermal resistance of ZSW (1.3×10^{-9} m^2K/W) at RT is much higher than that in ZS (5.5×10-10 m^2K/W), however, its value at 1800℃ only increased to 3.9×10^{-9} m^2K/W, slightly below that of ZS (4.2×10^{-9} m^2K/W). Although there are multiple grains and phases in ZS and ZSW, several randomly selected HRTEM prove that the GBs in both samples are clean (Fig. 3h and i). The detail TEM observations (Section 3.2) had previously verified that some glassy phase existed in the triangular grain boundary, but it only located in ZS. Therefore, according to the internal friction curve of ZS, softening of these glassy phases should take place during heating cycle and potentially rewets the adjacent the SiC/SiC and SiC/ZrB_2 GB at the same time. An EELS line scan clearly shows the aggregation of oxygen across one SiC/SiC grain boundary near the glassy phase, strongly supporting the existence of a glass rewet process. In fact, the rewetting process has been experimentally observed in several early publications [40,41]. It suppose that the isolation of conductive ZrB_2 or semiconductive SiC grains by glassy film with low conductivity (~1.0-1.6 W/(m·K) [42]) definitely cause the tremendous increase of interfacial thermal resistance, nevertheless, the process only dominates in the zone near the glassy phase. As calculated interfacial thermal

resistance reflects the averaged effect from all the GBs, hence, the value in ZSW is just slightly lower than that in ZS at 1800^{o}C.

By solution and grain refinement strengthening, the thermal conductivity of ceramics normally drops significantly at room temperature, due to the enhanced phonon scattering effects from the imperfections existed the specimen (impurity atoms, vacancies, dislocations, etc.) [12,43]. In this work, however, results indicate that effect is insignificant at high temperature when the contribution for thermal conductivity from phonon becomes dispensable. Moreover, removing the oxide based glassy phase in their microstructure by additives (e.g. WC) is critical and is an alternative route to further improve the thermal conductivity of ZrB_2 based Ultra-high Temperature Ceramics at ultra-high temperatures.

5. Conclusion

In summary, thermal, electrical property and damping behavior in hot-pressed ZrB_2-SiC (ZS) and ZrB_2-SiC-WC (ZSW) ceramics up to 1800^{o}C were investigated. Electrical resistivity increased linearly with temperature for both samples. At room temperature, the electrical conductivity value of ZS (8.13×10^6 S/m) is higher than that of ZSW (2.42×10^6 S/m), but they were approaching when temperature elevated. Seebeck coefficients of ZS and ZSW are negative, therefore, electron-like behavior dominates their electrical transport. Thermal conductivity of ZS (100.4 W/(m·K)) is nearly three times of ZSW (36.2 W/(m·K)) at room temperature. The values also differed in their temperature dependence: λ_{ZS} decreased continuously as temperature increased while λ_{ZSW} first increased then decreased within a narrow region between 36.2 and 45.1 W/(m·K) from RT to 1800^{o}C. Above 1400^{o}C, the contribution from lattice vibration on the overall thermal conductivity is neglectable. At room temperature, interfacial thermal resistance of ZSW is 2.4 times larger than that of ZS, while it becomes smaller than that in ZS at 1800^{o}C. HADDF with EDS and EELS verified that glassy phase existed in the triangular junction of ZS and corresponding internal friction curve also indicates the occurrence of glassy phase softening, which might rewet the adjacent SiC/SiC and SiC/ZrB_2 grain boundary during heating, as evidenced by a postmortem observation through EELS line scans. The significant drop of thermal

conductivity of ZS at higher temperature was ascribed to this process as well. At T>1400^{o}C, electrical conductivity dominated the thermal conductivity of ZS and ZSW ceramics, a clean grain boundary is helpful to further improve the thermal conductivity of UHTCs. In addition, the combination of excellent high temperature mechanical and thermal property of ZrB_2-SiC-WC makes it as a strong candidate for ablation resistant materials advanced by hypersonic flight.

Acknowledgements

The work was jointly supported financially by grants from the National Natural Science Foundation China (No. 51272266, 51532009 and 51672296), and an international collaboration program between Donghua University and University of Birmingham. The authors thank Prof Lidong Chen and Yuting Qin in Shanghai Institute of Ceramics, Chinese Academy of Sciences for providing the Seebeck coefficient and the electrical conductivity measurement.

Reference

[1] N.P. Padture. Advanced structural ceramics in aerospace propulsion, Nat. Mater. 15 (2016) 804-809.

[2] W.G. Fahrenholtz, G.E. Hilmas, I.G. Talmy, J.A. Zaykoski, Refractory diborides of zirconium and hafnium, J. Am. Ceram. Soc. 90 (2007) 1347-1364.

[3] F. Monteverde, R. Savino, Stability of ultra-high-temperature ZrB_2-SiC ceramics under simulated atmospheric re-entry conditions, J. Eur. Ceram. Soc. 27 (2007) 4797-4805.

[4] W.G. Fahrenholtz, G.E. Hilmas, Ultra-high temperature ceramics: Materials for extreme environments, Scripta Mater. 129 (2017) 94-99.

[5] J. Gild, Y. Zhang, T. Harrington, S. Jiang, T. Hu, M.C. Quinn, W.M. Mellor, N. Zhou, K. Vecchio, J. Luo, High-entropy metal diborides: A new class of high-entropy materials and a new type of ultrahigh temperature ceramics, Sci. Rep. 6 (2016) 37946-37946.

[6] A.L. Chamberlain, W.G. Fahrenholtz, G.E. Hilmas, Pressureless sintering of zirconium diboride, J. Am. Ceram. Soc. 89 (2006) 450-456.

[7] J. Zou, G.J. Zhang, Y.M. Kan, Formation of tough interlocking microstructure in ZrB_2-SiC-based ultrahigh-temperature ceramics by pressureless sintering, J. Mater. Res. 24 (2009) 2428-2434.

[8] S.C. Zhang, G.E. Hilmas, W.G. Fahrenholtz, Improved oxidation resistance of zirconium diboride by tungsten carbide additions, J. Am. Ceram. Soc. 91 (2008) 3530-3535.

[9] J. Zou, G.J. Zhang, C.F. Hu, T. Nishimura, Y. Sakka, J. Vleugels, O. Van der Biest, Strong ZrB_2-SiC-WC ceramics at 1600 degrees C, J. Am. Ceram. Soc. 95 (2012)

874-878.
[10] H.B. Ma, Z.Y. Man, J.X. Liu, F.F. Xu, G.J. Zhang, Microstructures, solid solution formation and high-temperature mechanical properties of ZrB_2 ceramics doped with 5vol.% WC, Mater. Design. 81 (2015) 133-140.
[11] F. Monteverde, L. Silvestroni, Combined effects of WC and SiC on densification and thermo-mechanical stability of ZrB2 ceramics, Mater. Design. 109 (2016) 396-407.
[12] D.L. McClane, W.G. Fahrenholtz, G.E. Hilmas, Thermal properties of (Zr,TM)B_2 solid solutions with TM = Hf, Nb, W, Ti, and Y, J. Am. Ceram. Soc. 97 (2014) 1552-1558.
[13] C. Richter, H.J. Viljoen, N.F.J. van Rensburg, Effective thermal conductivity estimates of particulate mixtures, J. Appl. Phys. 93 (2003) 2663-2670.
[14] S.C. Zhang, G.E. Hilmas, W.G. Fahrenholtz, Pressureless densification of zirconium diboride with boron carbide additions, J. Am. Ceram. Soc. 89 (2006) 1544-1550.
[15] J. Zou, S.K. Sun, G.J. Zhang, Y.M. Kan, P.L. Wang, T. Ohji, Chemical reactions, anisotropic grain growth and sintering mechanisms of self-reinforced ZrB_2-SiC doped with WC, J. Am. Ceram. Soc. 94 (2011) 1575-1583.
[16] J. Zou, G.J. Zhang, J. Vleugels, O. Van der Biest, High temperature strength of hot pressed ZrB_2–20vol% SiC ceramics based on ZrB_2 starting powders prepared by different carbo/boro-thermal reduction routes, J. Eur. Ceram. Soc. 33 (2013) 1609-1614.
[17] G. Roebben, L. Donzel, S. Stemmer, M. Steen, R. Schaller, O. Van der Biset, Viscous energy dissipation at high temperatures in silicon nitride, Acta Mater. 46 (1998) 4711-4723.
[18] R.G. Duan, G. Roebben, J. Vleugels, O. Van der Biest, In situ formation of Si_2N_2O and TiN in Si_3N_4-based ceramic composites, Acta Mater. 53 (2005) 2547-2554.
[19] L.F. He, Y.W. Bao, J.Y. Wang, M.S. Li, Y.C. Zhou, Microstructure and mechanical and thermal properties of ternary carbides in Hf–Al–C system, Acta Mater. 57 (2009) 2765-2774.
[20] R.D. Cowan, Pulse method of measuring thermal diffusivity at high temperatures, J. Appl. Phys. 34 (1963) 926-927.
[21] S. Guicciardi, A.K. Swarnakar, O. Van der Biest, D. Sciti, Temperature dependence of the dynamic Young's modulus of ZrB_2-$MoSi_2$ ultra-refractory ceramic composites, 62 (2010) 831-834.
[22] G. Grimvall. Thermophysical properties of materials, Enlarged and revised ed., Elsevier Science B.V., Amsterdam, 1999.
[23] J. Zou, G.J. Zhang, H. Zhang, Z. R. Huang, J. Vleugels, O. Van der Biest, Improving high temperature properties of hot pressed ZrB_2–20vol% SiC ceramic using high purity powders, Ceram. Int. 39 (2013) 871-876.
[24] M.J. Thompson, W.G. Fahrenholtz, G.E. Hilmas, N. Padture, Elevated temperature thermal properties of ZrB_2 with carbon additions, J. Am. Ceram. Soc. 95 (2012) 1077-1085.
[25] S. Fukuda, T. Kato, Y. Okamoto, H. Nakatsugawa, H. Kitagawa, S, Yamaguchi, Thermoelectric properties of single-crystalline SiC and dense sintered SiC for self-cooling devices, Jpn. J. Appl. Phys. 50 (2011) 031301.
[26] B. Fisher, K.B. Chashka, L. Patlagan, G.M. Reisner, Electronic transport in MgB_2, AlB_2 and ZrB_2 - a comparative study, Physica C. 384 (2003) 1-10.

[27] T. Ma, H. Li, X. Zheng, S.M. Wang, X.C. Wang, et al, H.Z. Zhao, S.B. Han, J, Liu, R.F. Zhang, P.W. Zhu, Y.W. Long, J.G. Cheng, Y.M. Ma, Y.S. Zhao, C.Q. Jin, X.H. Yu, Ultrastrong boron frameworks in ZrB_{12}: A highway for electron conducting, Adv. Mater. (2016), DOI: 10.1002/adma.201604003.

[28] L.D Zhao, S.H. Lo, J.Q. He, H. Li, K. Biswas, J. Androulakis, C.I. Wu, T.P. Hogan, D.Y. Chung, V.P. Dravid, High Performance Thermoelectrics from earth-abundant materials: enhanced figure of merit in PbS by second phase nanostructures, J. Am. Chem. Soc. 133 (2011) 20476-20487.

[29] G.J.K. Harrington, G.E. Hilmas, W.G. Fahrenholtz, Effect of carbon on the thermal and electrical transport properties of zirconium diboride, J. Eur. Ceram. Soc. 35 (2015) 887-896.

[30] M. Gasch, S. Johnson, J. Marschall, Thermal Conductivity Characterization of Hafnium Diboride-Based Ultra-High-Temperature Ceramics, J. Am. Ceram. Soc. 91 (2008) 1423-1432.

[31] M. Patel, V.V.B. Prasad, V. Jayaram, Heat conduction mechanisms in hot pressed ZrB_2 and ZrB_2–SiC composites, J. Eur. Ceram. Soc. 33 (2013) 1615-1624.

[32] L.N. Zhang, D.A. Pejakovic, J. Marschall, M. Gasch, Thermal and Electrical Transport Properties of Spark Plasma-Sintered HfB_2 and ZrB_2 Ceramics, J. Am. Ceram. Soc. 94 (2011) 2562-2570.

[33] M. Nakabayashi, T. Fujimoto, M. Sawamura, N. Ohtani, Silicon carbide single crystal, silicon carbide single crystal wafer, and method of production of same, US Patent No. 7,794,842 (2006)

[34] W.S. Williams, Transition metal carbides, nitrides, and borides for electronic applications, Jom-j. Min. Met. Mat. S. 49 (1997) 38-42.

[35] S. Okada, K. Kudou, T. Lundstrom, Preparations and some properties of W_2B, delta-WB and WB_2 crystals from high-temperature metal solutions, Jpn. J. Appl. Phys. 34 (1995) 226-231.

[36] Y. Goldberg, M.E. Levinshtein, S.L. Rumyantsev, Silicon carbide (SiC), In: M.E. Levinshtein, S.L. Rumyantsev, M.S. Shur (Eds.), Properties of advanced semiconductor materials GaN, AlN, SiC, BN, SiC, SiGe, John Wiley & Sons Inc., New York, 2001 pp. 93–148.

[37] H.O. Pierson, Handbook of refractory carbides and nitrides, First ed., William Andrew Inc., New York, 1996.

[38] O. Nilsson, H. Mehling, R. Horn, J. Fricke, R. Hofmann, S.G. Muller, R. Eckstein, D. Hofmann, Determination of the thermal diffusivity and conductivity of monocrystalline silicon carbide (300-2300 K), High Temp-high. Press 29 (1997) 73-79.

[39] R. Harrison, O. Ridd, D.D. Jayaseelan, W.E. Lee, Thermophysical characterisation of ceramics fabricated via carbothermic reduction–nitridation, J. Nucl. Mater. 454 (2014) 46-53.

[40] J. Luo, Y.M. Chiang, Existence and stability of nanometer-thick disordered films on oxide surfaces, Acta Mater. 48 (2000) 4501-4515.

[41] J. Luo, Y.M. Chiang, R.M. Cannon, Nanometer-thick surficial films in oxides as a case of prewetting, Langmuir. 21 (2005) 7358-7365.

[42] M. Susa, M. Watanabe, S. Ozawa, R. Endo, Thermal conductivity of $CaO\text{-}SiO_2\text{-}Al_2O_3$

glassy slags: Its dependence on molar ratios of Al_2O_3/CaO and SiO_2/Al_2O_3, Ironmak. Steelmak. 34 (2007) 124-130.

[43] D.L. McClane, W.G. Fahrenholtz, G.E. Hilmas, D. Smith, Thermal properties of (Zr, TM)B_2 solid solutions with TM = Ta, Mo, Re, V, and Cr, J. Am. Ceram. Soc. 98 (2015) 637-644.

Figure captions

Fig. 1 Polished surfaces of ZS (a) and ZSW (b), the corresponding EDS patterns marked 1-4 in 1b were also presented.

Fig. 2 XRD patterns of ZSW ceramics using Si as a reference (a), the shifting of ZrB_2 peak towards higher angles are shown in 2b.

Fig. 3 HAADF image of ZS (a) and corresponding EDS (b) and EELS (c) spectrum of a triangular grain boundary circled in ZS; EELS line scan of O signal (k edge) of the GBs in ZS(d and e) and ZSW (j and k); (f) O, Ca, Al, Si elemental mappings of the main impurities presented in 3a or d; (g) HRTEM of the amorphous phase; Typical HRTEM of clean ZrB_2/ZrB_2 GBs in ZS (h) and ZSW (i).

Fig. 4 Thermal diffusivity (a), specific heat capacity (b) of ZS, ZSW samples; thermal conductivity, contributions of electron and phonon to the total thermal conductivity for ZS (c) and ZSW (d). The specific heat capacity of ZS and ZSW above 1400^{o}C was calculated according to the fitting of measured values from room temperature to 1400^{o}C.

Fig. 5 Electrical resistivity and electrical conductivity (a), Seebeck coefficient (b) and *zT* values (c) of ZS and ZSW, as a function of temperatures. The electrical resistivity of ZS and ZSW above 700^{o}C was calculated according to the fitting of measured values from room temperature to 700^{o}C.

Fig. 6 Calculated true Lorenz number of ZS and ZSW from 25 to 500^{o}C.

Fig. 7 Damping curves of ZS and ZSW during heating and cooling.

Fig. 8 Cross section image of ZSW after IET and corresponding O, C, Zr, Si, B, W elemental mapping by WDS.

Fig. 9 GIXRD results of ZSW surfaces after the IET test with different incident angles (Ω) from 0.5 to 3 degree.

Table captions

Table I. Electrical and Thermal conductivity values of ZrB_2, SiC, ZrC and WB.

Table II. Interfacial electrical (R_σ) and thermal (R_λ) resistance of ZS and ZSW.

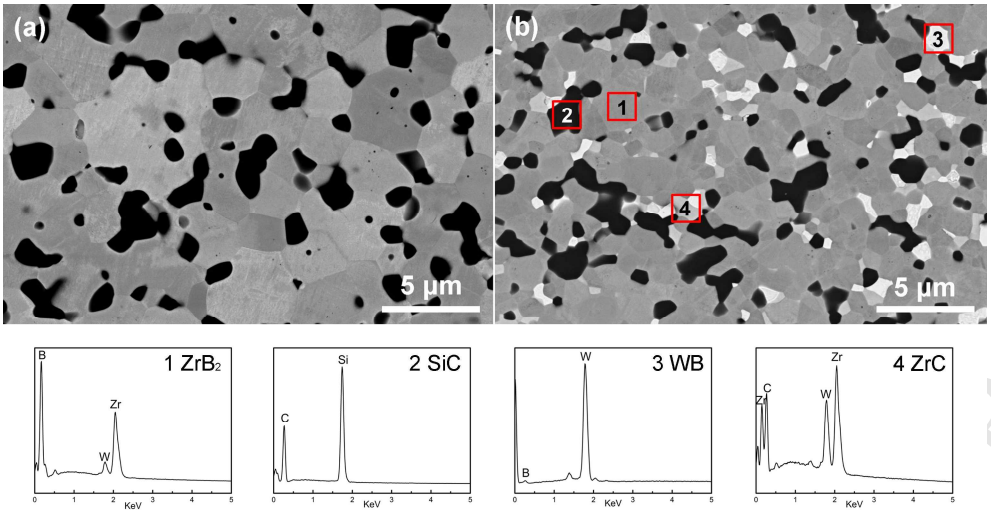

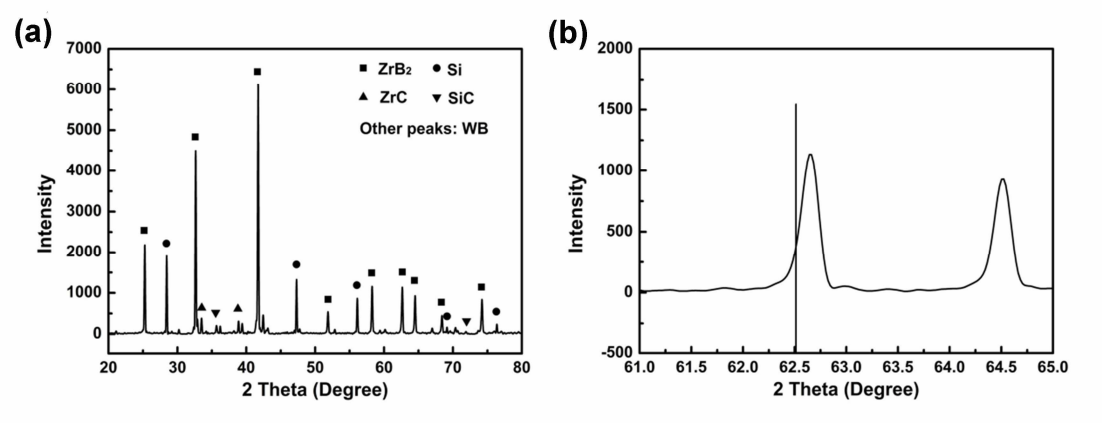

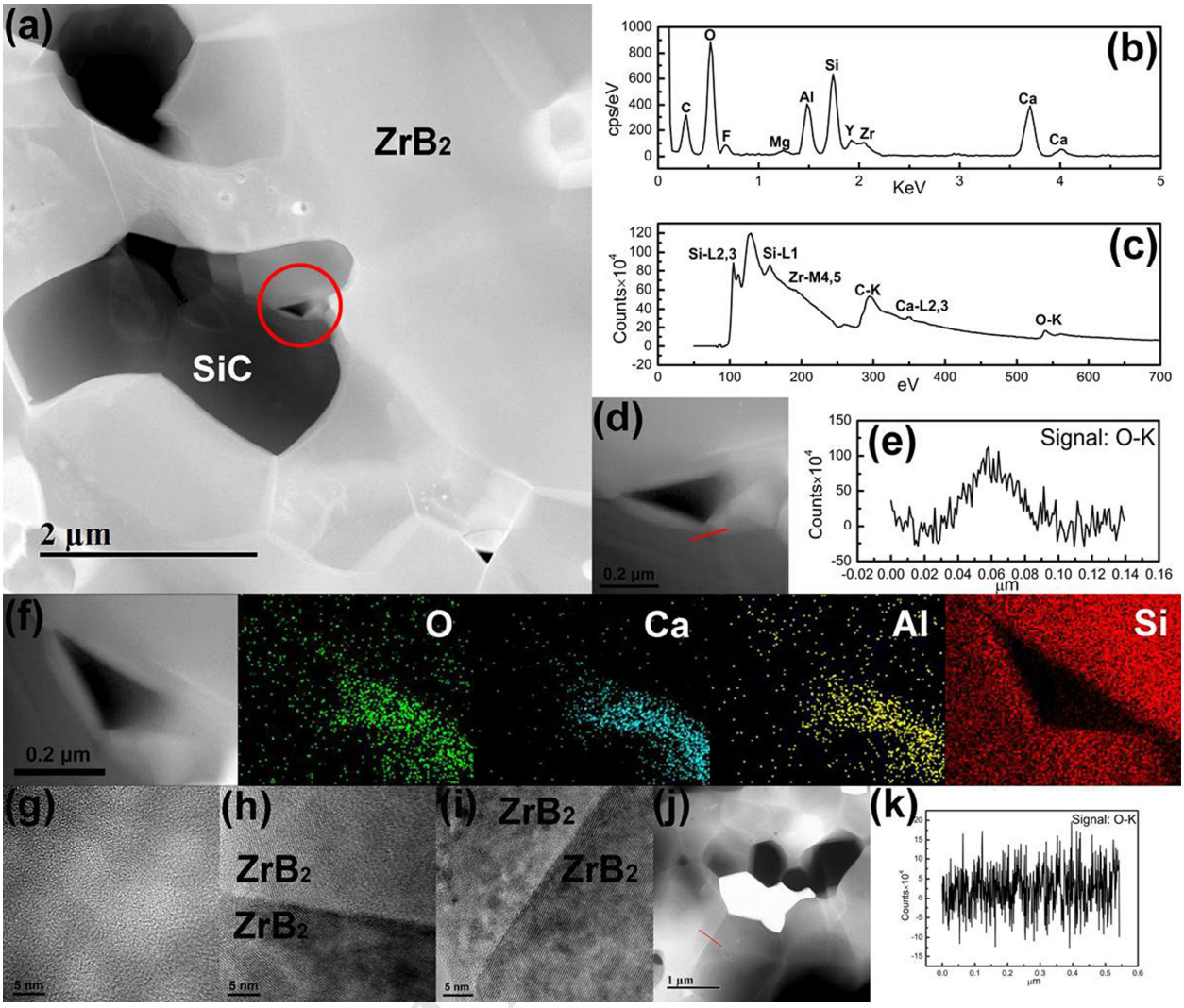
(a)
ZrB2
SiC
2 μm
(b)
cps/eV
KeV
O
C
F
Mg
Al
Si
Y
Zr
Ca
Ca
(c)
Counts×10^4
eV
Si-L2,3
Si-L1
Zr-M4,5
C-K
Ca-L2,3
O-K
(d)
0.2 μm
(e)
Signal: O-K
Counts×10^4
μm
(f)
0.2 μm
O
Ca
Al
Si
(g)
5 nm
(h)
ZrB2
ZrB2
5 nm
(i)
ZrB2
ZrB2
5 nm
(j)
1 μm
(k)
Signal: O-K
Counts×10^4
μm

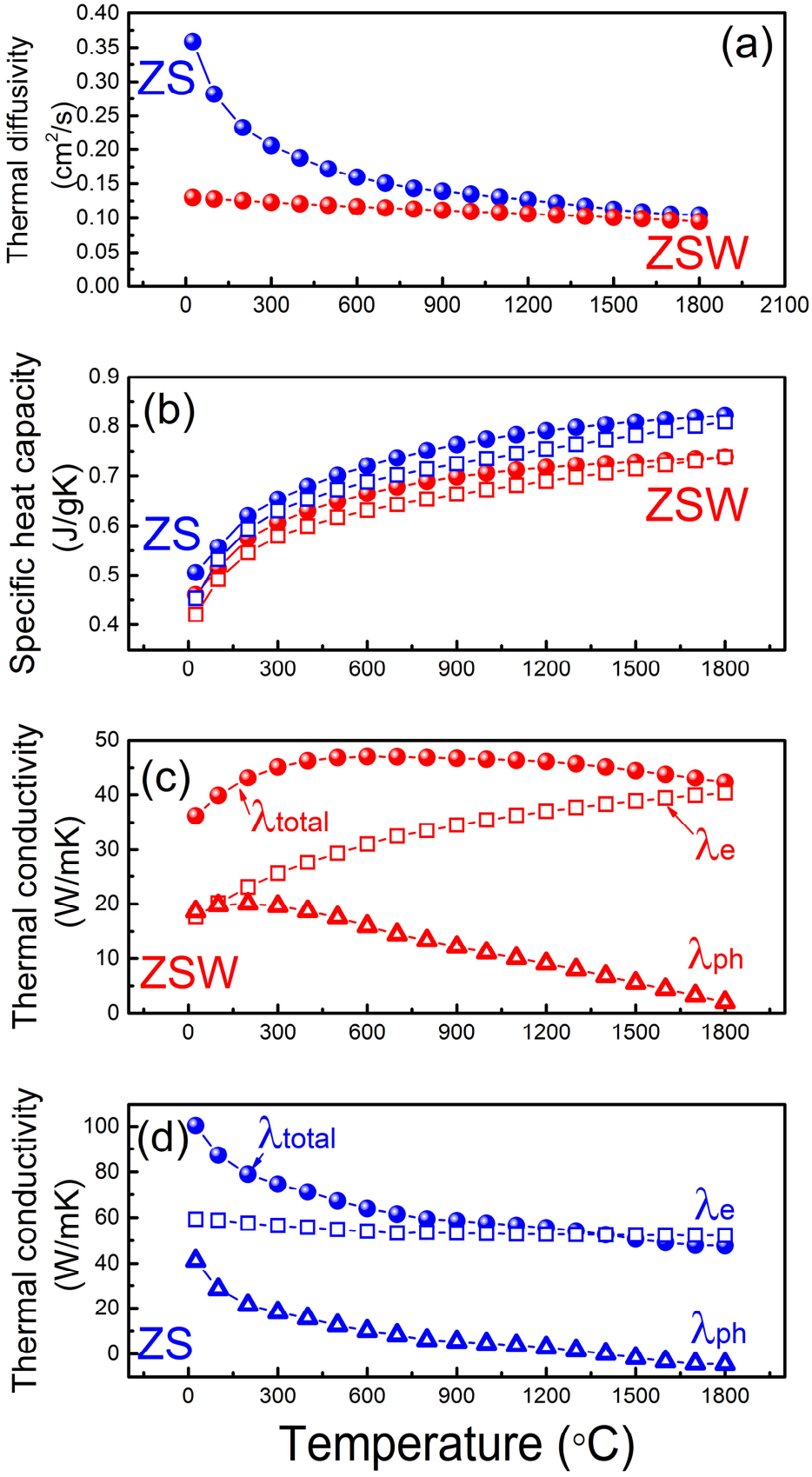
(a)
ZS
ZSW
Thermal diffusivity (cm²/s)
0.40
0.35
0.30
0.25
0.20
0.15
0.10
0.05
0.00
0
300
600
900
1200
1500
1800
2100
(b)
ZS
ZSW
Specific heat capacity (J/gK)
0.9
0.8
0.7
0.6
0.5
0.4
0
300
600
900
1200
1500
1800
(c)
λtotal
λe
λph
ZSW
Thermal conductivity (W/mK)
50
40
30
20
10
0
0
300
600
900
1200
1500
1800
(d)
λtotal
λe
λph
ZS
Thermal conductivity (W/mK)
100
80
60
40
20
0
0
300
600
900
1200
1500
1800
Temperature (◦C)

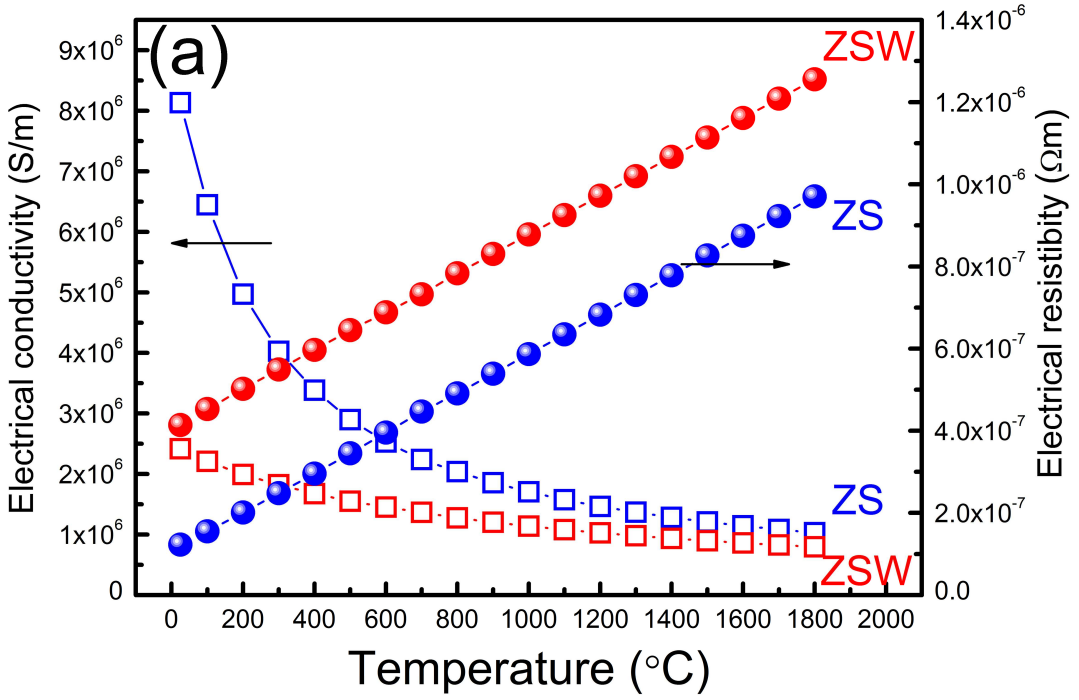
(a)
ZSW
ZS
ZS
ZSW
Electrical conductivity (S/m)
Electrical resistibity (Ωm)
Temperature (°C)
0
1x10^6
2x10^6
3x10^6
4x10^6
5x10^6
6x10^6
7x10^6
8x10^6
9x10^6
2.0x10^-7
4.0x10^-7
6.0x10^-7
8.0x10^-7
1.0x10^-6
1.2x10^-6
1.4x10^-6
0.0
0
200
400
600
800
1000
1200
1400
1600
1800
2000

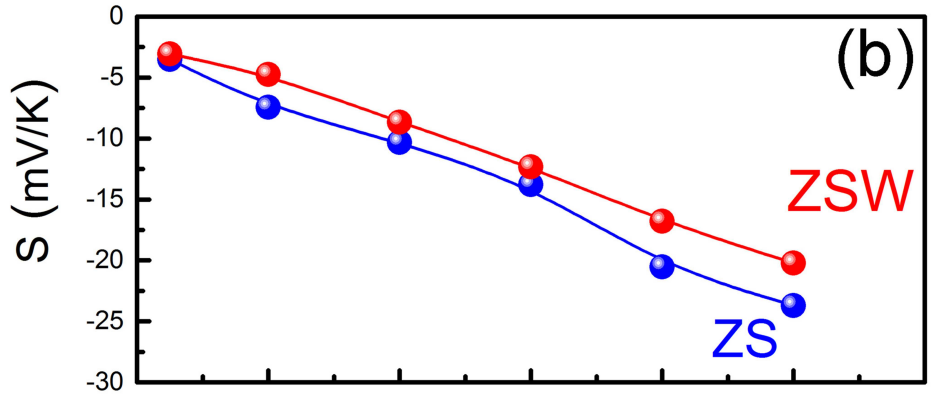
(b)
ZSW
ZS
S (mV/K)
0
-5
-10
-15
-20
-25
-30

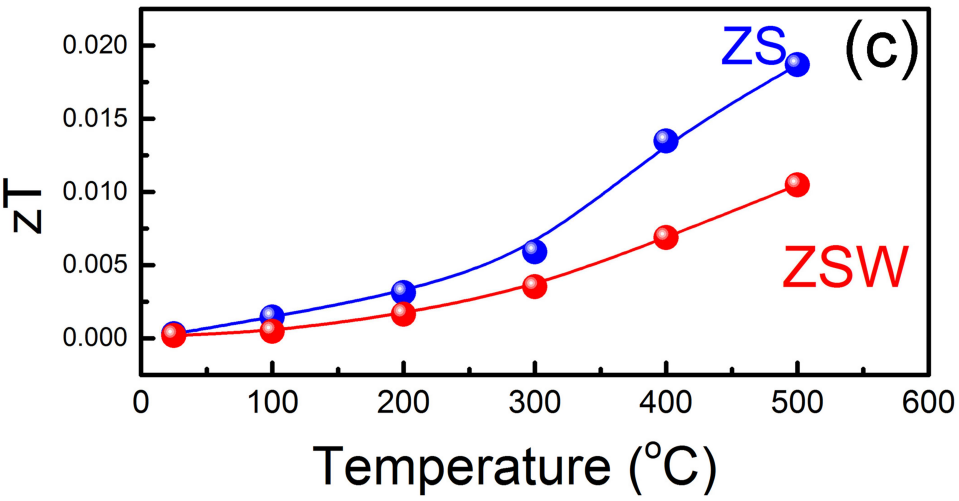
(c)
ZS
ZSW
zT
Temperature (°C)
0.000
0.005
0.010
0.015
0.020
0
100
200
300
400
500
600

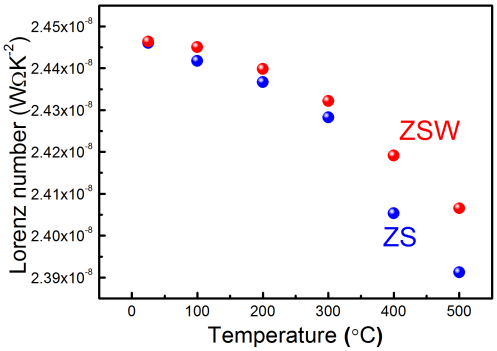

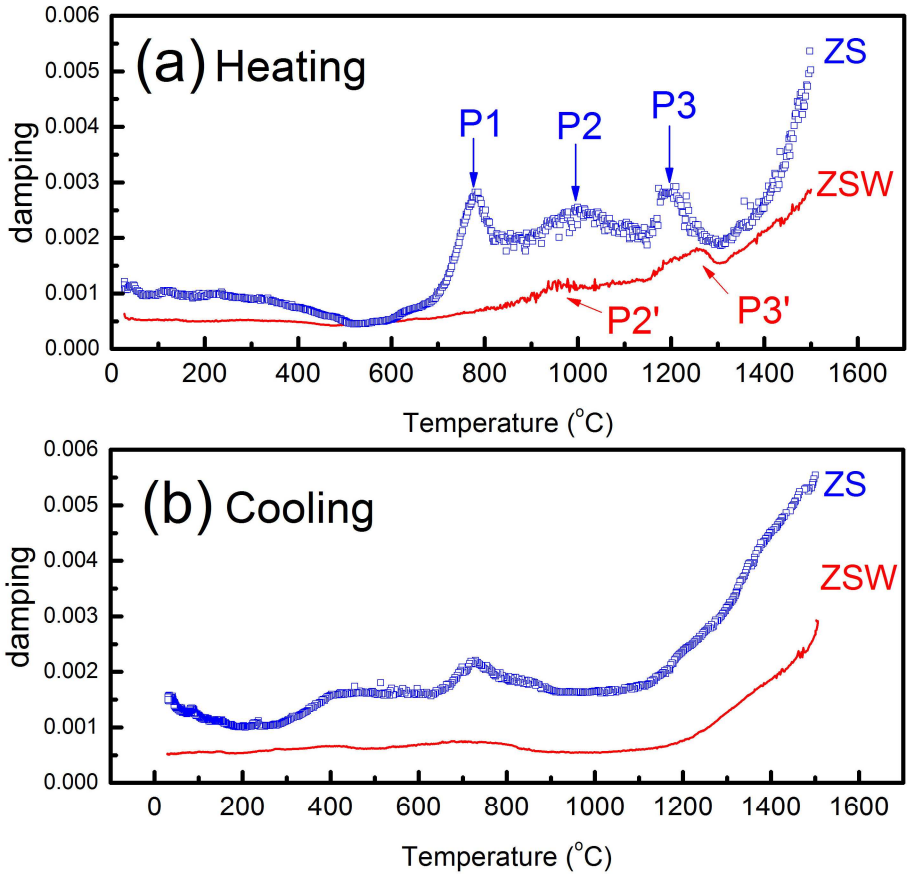

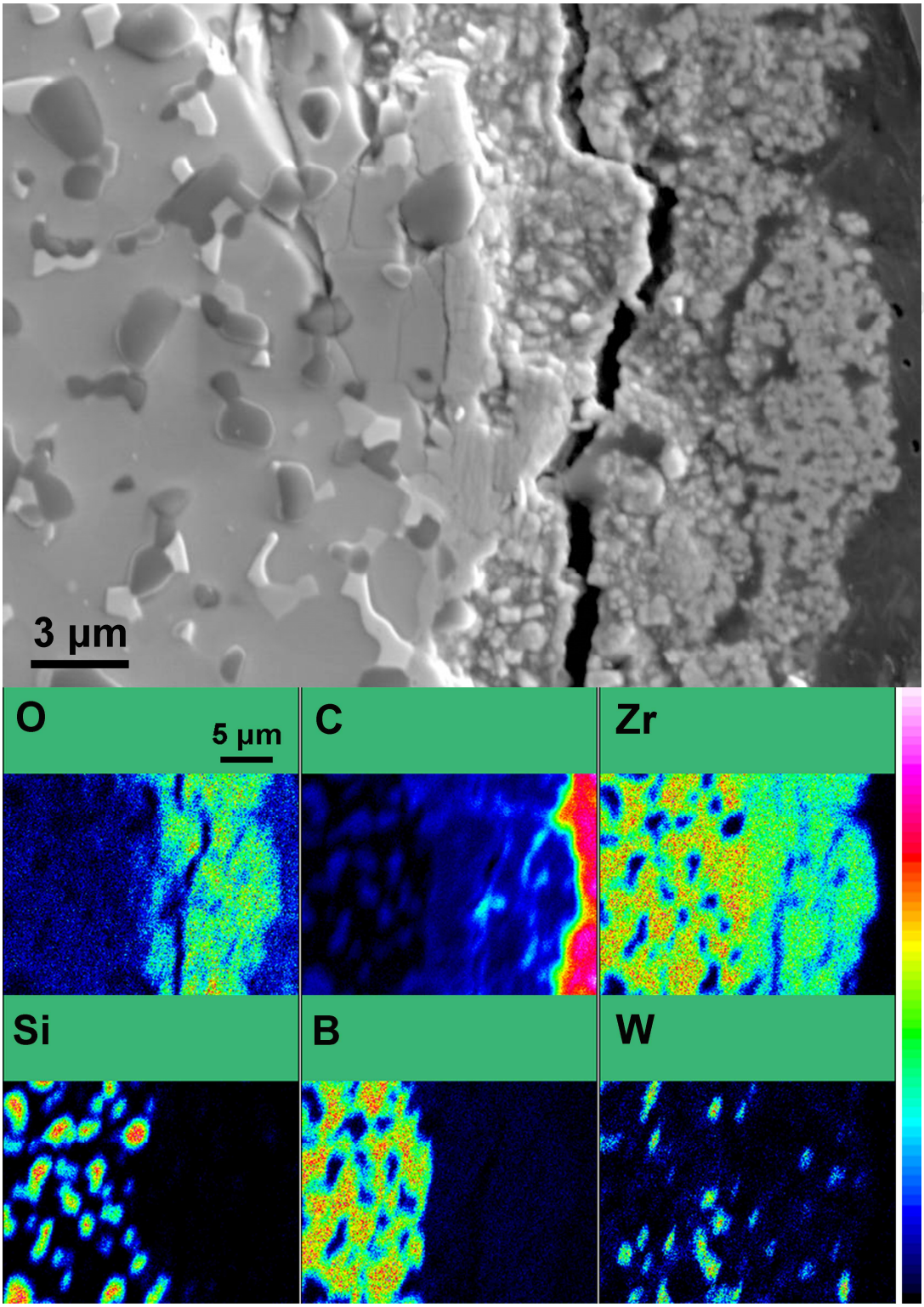
3 µm
O
5 µm
C
Zr
Si
B
W